Exact Analysis of the Wire-Bonded Multiconductor Transmission Line

Juan E. Page, Enrique Márquez-Segura, *Senior Member, IEEE*, Francisco P. Casares-Miranda, *Student Member, IEEE*, Jaime Esteban, Pablo Otero, *Member, IEEE*, and Carlos Camacho-Peñalosa, *Member, IEEE*

***Abstract*—In this paper, the exact model of a multiconductor transmission line with bonding wires is presented. The model is based on the multiport admittance matrix, and is valid for any number of conductors in the structure. The model shows how to compute the two-port admittance matrix of the wire-bonded structure with direct application to the wire-bonded interdigital capacitor. The model has been validated by means of method-of-moments-based numerical simulation and by experimental work.**

***Index Terms*—Interdigital capacitor, microwave integrated circuits, microwave passive circuits, multiconductor transmission lines, wire-bonded interdigital capacitor, wire bonding.**

I. Introduction

MICROSTRIP interdigital capacitors have been improved by the connection of bonding wires across the open ends of the capacitor fingers [1], as sketched in Fig. 1. The resulting device is the so-called wire-bonded interdigital capacitor. This device has several advantages over the conventional interdigital capacitor: the undesired resonances at higher frequencies are removed, which results in a larger bandwidth of operation, and there is a slight increment in nominal capacitance. A recent application of the wire-bonded interdigital capacitor can be found in [2]. Of course, the process of connecting bonding wires across the open ends of the fingers of the interdigital capacitor is cumbersome. An analytical model of the wire-bonded interdigital capacitor has been recently published [3]. Nevertheless, this device can be considered as well, i.e., a rectilinear multiconductor guiding structure in a heterogeneous dielectric.

In this paper, the exact analysis of a multiconductor guiding structure with short-circuited alternate conductors is presented. The analysis, which is based on the multiport admittance matrix, is derived in Section II. The model is valid for any number of coupled transmission lines, even or odd. Particular equations for homogeneous and heterogeneous lossless dielectrics have been obtained and presented, respectively, in Sections III and IV. Section V deals with the analysis validation by means of both numerical simulations using a full-wave computer program based on the method of moments (MoM) and by experimental work.

Manuscript received August 9, 2006; revised May 10, 2007. This work was supported by the Spanish Ministry of Education and Science and by the European Union under European Regional Development Funds Project TEC2006-04771.

J. E. Page and J. Esteban are with the Departamento Electromagnetismo y Teoría de Circuitos, Escuela Técnica Superior de Ingenieros de Telecomunicación, Universidad Politécnica de Madrid, 28040 Madrid, Spain (e-mail: jep@etc.upm.es).

E. Márquez-Segura, F. P. Casares-Miranda, Pablo Otero, and C. Camacho-Peñalosa are with the Departamento Ingeniería de Comunicaciones, Escuela Técnica Superior de Ingeniería de Telecomunicación, Universidad de Málaga, 29071 Málaga, Spain (e-mail: ems@ic.uma.es).

Color versions of one or more of the figures in this paper are available online at http://ieeexplore.ieee.org.

Digital Object Identifier 10.1109/TMTT.2007.902084

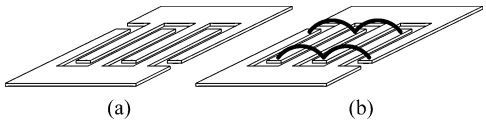

Fig. 1. (a) Interdigital capacitor. (b) Wire-bonded interdigital capacitor.

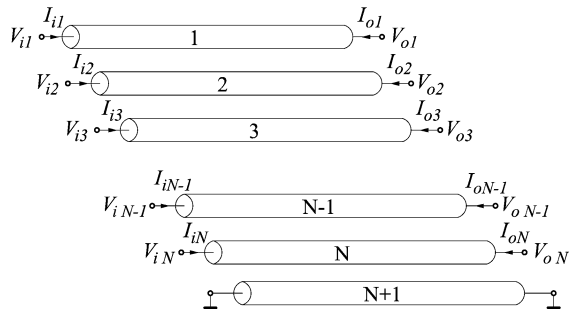

Fig. 2. Multiconductor guiding structure.

II. Exact Analysis of the Wire-Bonded Interdigital Capacitor

Consider a finite length guiding structure consisting of $N+1$ conductors, as shown in Fig. 2. It is not necessary that all the conductors have the same shape in the transversal plane. This structure can propagate N TEM modes in the homogeneous dielectric case or N quasi-TEM modes in the heterogeneous case. Without loss of generality, one of the conductors, i.e., the conductor numbered $N+1$, can be considered the voltage reference. Voltages and currents at both ends of the N conductors are related through the admittance matrix equation

$$\bar{I} = [Y]\bar{V} \tag{1}$$

where $\bar{V}$ and $\bar{I}$ are vectors of length $2N$, their elements being the voltages and currents at both ends of the circuit of Fig. 2 as follows:

$$\bar{V} = [V_{i1}, V_{i2}, \ldots, V_{iN}, V_{o1}, V_{o2}, \ldots, V_{oN}]^T \tag{2}$$

$$\bar{I} = [I_{i1}, I_{i2}, \ldots, I_{iN}, I_{o1}, I_{o2}, \ldots, I_{oN}]^T \tag{3}$$

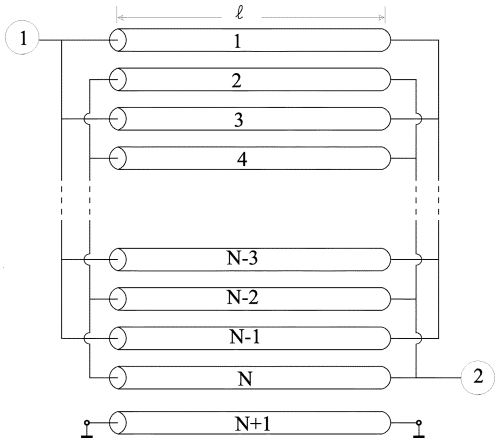

Fig. 3. Multiconductor transmission line structure of the wire-bonded interdigital capacitor.

where superscript T denotes transpose. The admittance matrix is square of dimension $2N \times 2N$ as follows:

$$[Y] = \begin{bmatrix} Y_{11} & Y_{12} & \cdots & Y_{1,2N} \\ Y_{21} & Y_{22} & \cdots & Y_{2,2N} \\ \vdots & \vdots & \ddots & \vdots \\ Y_{2N,1} & Y_{2N,2} & \cdots & Y_{2N,2N} \end{bmatrix}. \tag{4}$$

When the ends of the odd-numbered conductors are connected on one side of the structure, and the ends of the even-numbered conductors are connected on the opposite side, as shown in Fig. 1(a), an interdigital capacitor is obtained, and the following conditions apply:

$$\begin{aligned} &V_{i1} = V_{i3} = V_{i5} = \cdots = V_{iN} = V_i \\ &V_{o2} = V_{o4} = V_{o6} = \cdots = V_{oN} = V_o \end{aligned} \tag{5a}$$

$$\begin{aligned} &I_{i1} + I_{i3} + I_{i5} + \cdots + I_{iN} \\ &\quad = I_i \\ &I_{o2} + I_{o4} + I_{o6} + \cdots + I_{oN} \\ &\quad = I_o \end{aligned} \tag{5b}$$

when N is odd and four equations similar to (5a) and (5b) when N is even.

If the fingers of the interdigital capacitor are now connected together on the open end using bonding wires, as shown in Fig. 1(b), the multiconductor structure shown in Fig. 2 becomes that of Fig. 3 (the so-called wire-bonded interdigital capacitor), and additional constraints on voltages and currents are imposed as follows:

$$\begin{aligned} &V_{i2} = V_{i4} = V_{i6} = \cdots = V_{iN-1} \\ &V_{o1} = V_{o3} = V_{o5} = \cdots = V_{oN} \end{aligned} \tag{6a}$$

$$\begin{aligned} &I_{i2} + I_{i4} + I_{i6} + \cdots + I_{iN-1} \\ &\quad = 0 \\ &I_{o1} + I_{o3} + I_{o5} + \cdots + I_{oN} \\ &\quad = 0 \end{aligned} \tag{6b}$$

when N is odd and four equations similar to (6a) and (6b) for the case of N are even.

The wire-bonded interdigital capacitor is a two-port device, therefore, (1) becomes

$$\begin{bmatrix} I_i \\ I_o \end{bmatrix} = \begin{bmatrix} y_{11} & y_{12} \\ y_{21} & y_{22} \end{bmatrix} \begin{bmatrix} V_i \\ V_o \end{bmatrix} = [y] \begin{bmatrix} V_i \\ V_o \end{bmatrix} \tag{7}$$

where $[y]$ is the two-port admittance matrix, given by

$$[y] = \left[y^{(1)}\right] - \left[y^{(2)}\right] \left[y^{(3)}\right]^{-1} \left[y^{(2)}\right]^T \tag{8}$$

and the matrices $[y^{(i)}]$, $i = 1, 2, 3$ are obtained by means of the following equations, depending on the number of fingers of the wire-bonded interdigital capacitor.

1) N even

$$\begin{aligned} y_{11}^{(1)} &= \sum_{i=1}^{N-1} \sum_{j=1}^{N-1} Y_{ij}, \qquad i,\ j \text{ odd} \\ y_{12}^{(1)} = y_{21}^{(1)} &= \sum_{i=1}^{N-1} \sum_{j=N+2}^{N+N} Y_{ij}, \qquad i \text{ even};\quad j \text{ odd} \\ y_{22}^{(1)} &= \sum_{i=N+2}^{N+N} \sum_{j=N+2}^{N+N} Y_{ij}, \qquad i,\ j \text{ even} \end{aligned} \tag{9}$$

$$\begin{aligned} y_{11}^{(2)} &= \sum_{i=1}^{N-1} \sum_{j=2}^{N} Y_{ij}, \qquad i \text{ odd};\quad j \text{ even} \\ y_{12}^{(2)} &= \sum_{i=1}^{N-1} \sum_{j=N+1}^{N+N-1} Y_{ij}, \qquad i,\ j \text{ odd} \\ y_{21}^{(2)} &= \sum_{i=N+2}^{N+N} \sum_{j=2}^{N} Y_{ij}, \qquad i,\ j \text{ even} \\ y_{22}^{(2)} &= \sum_{i=N+2}^{N+N} \sum_{j=N+1}^{N+N-1} Y_{ij}, \qquad i \text{ even};\quad j \text{ odd} \end{aligned} \tag{10}$$

$$\begin{aligned} y_{11}^{(3)} &= \sum_{i=2}^{N} \sum_{j=2}^{N} Y_{ij}, \qquad i,\ j \text{ even} \\ y_{12}^{(3)} = y_{21}^{(3)} &= \sum_{i=2}^{N} \sum_{j=N+1}^{N+N-1} Y_{ij}, \qquad i \text{ even};\quad j \text{ odd} \\ y_{22}^{(3)} &= \sum_{i=N+1}^{N+N-1} \sum_{j=N+1}^{N+N-1} Y_{ij}, \qquad i,\ j \text{ odd}. \end{aligned} \tag{11}$$

2) N odd

$$\begin{aligned} y_{11}^{(1)} &= \sum_{i=1}^{N} \sum_{j=1}^{N} Y_{ij}, \qquad i,\ j \text{ even} \\ y_{12}^{(1)} = y_{21}^{(1)} &= \sum_{i=1}^{N} \sum_{j=N+2}^{N+N-1} Y_{ij}, \qquad i,\ j \text{ even} \\ y_{22}^{(1)} &= \sum_{i=N+2}^{N+N-1} \sum_{j=N+1}^{N+N-1} Y_{ij}, \qquad i,\ j \text{ even} \\ y_{11}^{(2)} &= \sum_{i=1}^{N} \sum_{j=2}^{N-1} Y_{ij}, \qquad i \text{ odd};\quad j \text{ even} \end{aligned} \tag{12}$$

$$y_{12}^{(2)} = \sum_{i=1}^{N}\sum_{j=N+1}^{N+N} Y_{ij}, \qquad i \text{ odd}; \quad j \text{ even}$$
$$y_{21}^{(2)} = \sum_{i=N+2}^{N+N-1}\sum_{j=2}^{N-1} Y_{ij}, \qquad i \text{ odd}; \quad j \text{ even}$$
$$y_{22}^{(2)} = \sum_{i=N+2}^{N+N-1}\sum_{j=N+1}^{N+N} Y_{ij}, \qquad i \text{ odd}; \quad j \text{ even} \tag{13}$$
$$y_{11}^{(3)} = \sum_{i=2}^{N-1}\sum_{j=2}^{N-1} Y_{ij}, \qquad i,\ j \text{ even}$$
$$y_{12}^{(3)} = y_{21}^{(3)} = \sum_{i=2}^{N-1}\sum_{j=N+1}^{N+N} Y_{ij}, \qquad i,\ j \text{ even}$$
$$y_{22}^{(3)} = \sum_{i=N+1}^{N+N}\sum_{j=N+1}^{N+N} Y_{ij}, \qquad i,\ j \text{ even.} \tag{14}$$

Equations (9)–(14) show that once the admittance matrix $[Y]$ in (4) is known, the two-port admittance $[y]$ in (8) can be calculated. The admittance matrix $[Y]$ for the lossless homogeneous and heterogeneous dielectric cases are obtained below, but the presence of moderate losses hardly changes either the algebra or the results [4].

III. Homogeneous Lossless Dielectric

Providing the dielectric around the conductors in Fig. 2 is homogeneous and lossless, N TEM modes will be supported by the guiding structure and the admittance matrix can be written as [5]

$$[Y] = -j\begin{bmatrix} [Y_0]\cot(\beta_0\ell) & -[Y_0]\csc(\beta_0\ell) \\ -[Y_0]\csc(\beta_0\ell) & [Y_0]\cot(\beta_0\ell) \end{bmatrix} \tag{15}$$

where $\beta_0 = \omega\sqrt{\mu\varepsilon}$ is the phase constant of all the TEM modes, ℓ is the length of the fingers, and $[Y_0] = [C]/\sqrt{\mu\varepsilon}$ is the characteristic admittance matrix of dimension $N \times N$, where $[C]$ is the static capacitance matrix per unit length.

Using (9)–(15), the two-port admittance matrix in (8) can be obtained as

$$[y] = \frac{-j}{\sqrt{\mu\varepsilon}}\frac{c_{11e}\,c_{22e} - c_{12e}^2}{(c_{11e}c_{22e} - c_{12e}^2)\csc^2(\beta_0\ell) - c_{11e}c_{22e}} \cdot \begin{bmatrix} c_{11e}\cot(\beta_0\ell) & c_{12e}\csc(\beta_0\ell) \\ c_{12e}\csc(\beta_0\ell) & c_{22e}\cot(\beta_0\ell) \end{bmatrix} \tag{16}$$

where the c_{ije} coefficients are given, for N even, by

$$c_{11e} = \sum_{i=1}^{N-1}\sum_{j=1}^{N-1} c_{ij}, \qquad i,\ j \text{ odd}$$
$$c_{12e} = c_{21e} = \sum_{i=1}^{N-1}\sum_{j=N+2}^{N+N} c_{ij}, \qquad i \text{ odd}; \quad j \text{ even}$$
$$c_{22e} = \sum_{i=N+2}^{N+N-1}\sum_{j=N+2}^{N+N-1} c_{ij}, \qquad i,\ j \text{ even} \tag{17}$$

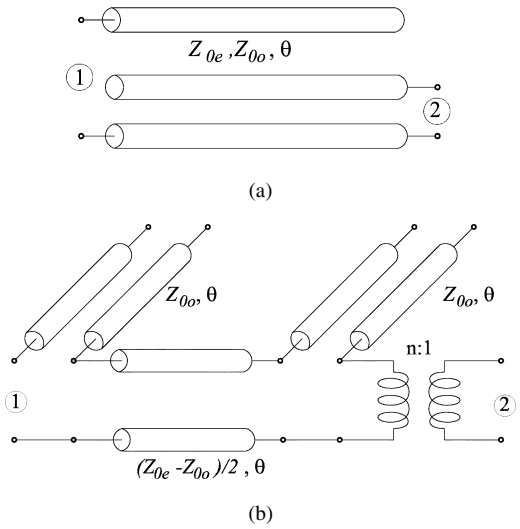

Fig. 4. (a) Pair of coupled lines in bandpass filter configuration. (b) Equivalent circuit.

and, for N odd, by

$$c_{11e} = \sum_{i=1}^{N}\sum_{j=1}^{N} c_{ij}, \qquad i,\ j \text{ odd}$$
$$c_{12e} = c_{21e} = \sum_{i=1}^{N}\sum_{j=N+2}^{N+N-1} c_{ij}, \qquad i,\ j \text{ odd}$$
$$c_{22e} = \sum_{i=N+2}^{N+N}\sum_{j=N+2}^{N+N} c_{ij}, \qquad i,\ j \text{ odd.} \tag{18}$$

A. Equivalent Circuit of the Structure

The matrix $[y]$ obtained in (16) is the admittance matrix of two coupled lines in the bandpass filter configuration, as shown in Fig. 4(a) [6]. The static capacitance coefficients of that cell are those obtained with (17) or (18), and the equivalent circuit is shown in Fig. 4(b) [7]. The values of the characteristic impedances, and the voltage transform ratio, are given by

$$Z_{0e} = \frac{\sqrt{\mu\varepsilon}}{c_e}$$
$$Z_{0o} = \frac{\sqrt{\mu\varepsilon}}{c_o} \tag{19}$$
$$n = \sqrt{\frac{c_{22e}}{c_{11e}}} \tag{20}$$

and the coefficients c_e and c_o are given by

$$c_e = c_{11e} + \frac{1}{n}c_{12e}$$
$$c_o = c_{11e} - \frac{1}{n}c_{12e}. \tag{21}$$

The behavior of the circuit shown in Fig. 4 can be qualitatively determined by means of a couple of examples. Consider

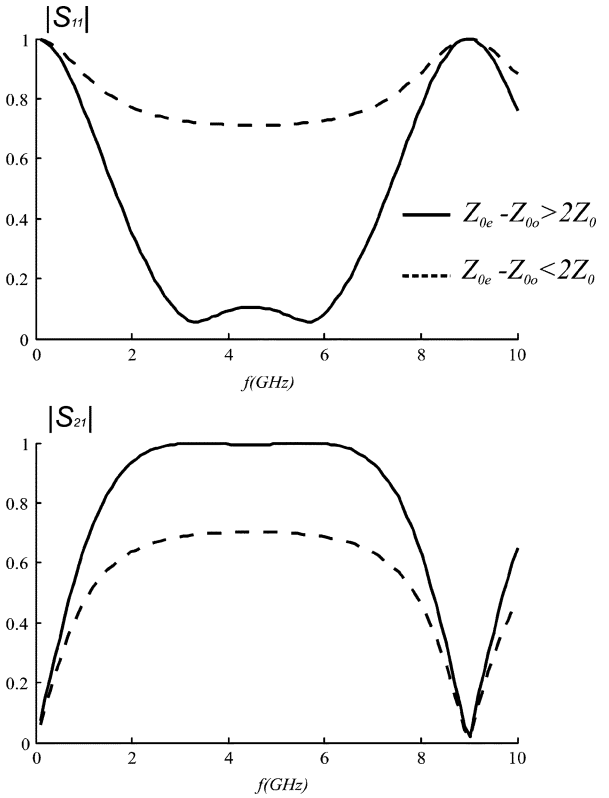

Fig. 5. Scattering matrix elements of the coupled line bandpass filter section.

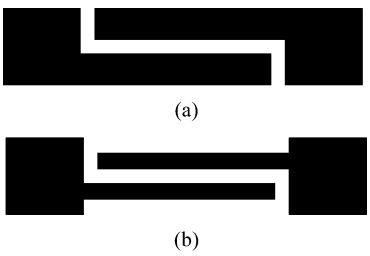

Fig. 6. Two coupled line bandpass filter sections.

two multiconductor circuits of equal length. Fig. 5 shows the magnitudes of the scattering elements when both circuits are loaded with the reference impedance Z_0. When $Z_{0e} - Z_{0o} < 2Z_0$, a single minimum is obtained, but not a reflection zero. On the other hand, if $Z_{0e} - Z_{0o} > 2Z_0$, then two reflection zeros are obtained. Which case corresponds to a particular structure? It should be noted that, in the case of two coupled striplines with a total width equal to that of the connecting stripline, as shown in Fig. 6(a) (even if the two fingers had unequal widths), it always happens that $Z_{0e} - Z_{0o} < 2\,Z_c$, where Z_c is the characteristic impedance of the connecting stripline. Only when the connecting stripline is wider than the coupled pair, as in Fig. 6(b), the condition $Z_{0e} - Z_{0o} > 2\,Z_c$ can be fulfilled.

Obviously, the performance of a wire-bonded interdigital capacitor depends on its geometry. Nevertheless, in all the cases analyzed thus far, the behavior stated above has been found. A structure of the same width or wider than the stripline has to be used if the desired response is that of the dashed line in Fig. 5, but, if the desired response is that of the solid line in Fig. 5 (e.g., when a wideband dc coupling capacitor is to be designed), a capacitor narrower than the stripline could be necessary. Some results confirming that behavior in microstrip wire-bonded interdigital capacitors are included in Section V.

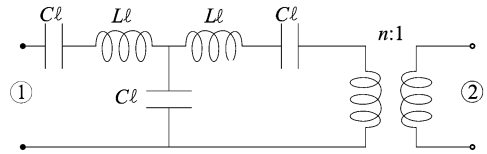

Fig. 7. Low-frequency equivalent circuit of Fig. 4.

B. Electrically Short Multiconductor Structure

When the conductors are electrically short, i.e., when

$$\theta = \beta\ell \ll 1 \tag{22}$$

where θ is the electrical length shown in Fig. 4, the equivalent circuit is simplified to that shown in Fig. 7. The values of the elements in Fig. 7 are

$$L = \frac{1}{2}\mu\varepsilon\frac{c_e + c_o}{x2\,c_e\,c_o} \tag{23a}$$

$$C = \frac{2c_e c_o}{c_o - c_e} \tag{23b}$$

and the approximation obtained by means of this simplified circuit is accurate up to frequencies where the length ℓ is smaller than one-eighth of the guided wavelength.

IV. Heterogeneous Lossless Dielectric Case

When the multiconductor structure is built with a heterogeneous lossless dielectric, the quasi-TEM modes are described by means of the eigenvalues and eigenvectors of the matrix $[C_0]^{-1}[C]$, where $[C]$ is the static capacitance matrix per unit length, and $[C_0]$ is the same matrix of the multiconductor line in free space [8]. The eigenvalues of that matrix are the effective permittivities corresponding to each single mode. The admittance matrix can be computed by means of the following relation:

$$[Y] = 2\begin{bmatrix}[Y_A] & [Y_B]\\ [Y_B] & [Y_A]\end{bmatrix} \tag{24}$$

with

$$\begin{aligned}[Y_A] &= [[v]^{-1}]^T \operatorname{diag}(-j\cot\beta_i\ell)[v]^{-1}\\ [Y_B] &= -[[v]^{-1}]^T \operatorname{diag}(-j\csc\beta_i\ell)[v]^{-1}\end{aligned} \tag{25}$$

where $[v]$ is the matrix of eigenvectors arranged in columns, and ℓ is the length of the multiconductor structure.

Any quasi-TEM mode has a different phase constant and no simple equivalent circuit seems to exist, but an approximation is possible if a single phase velocity is used for all modes.

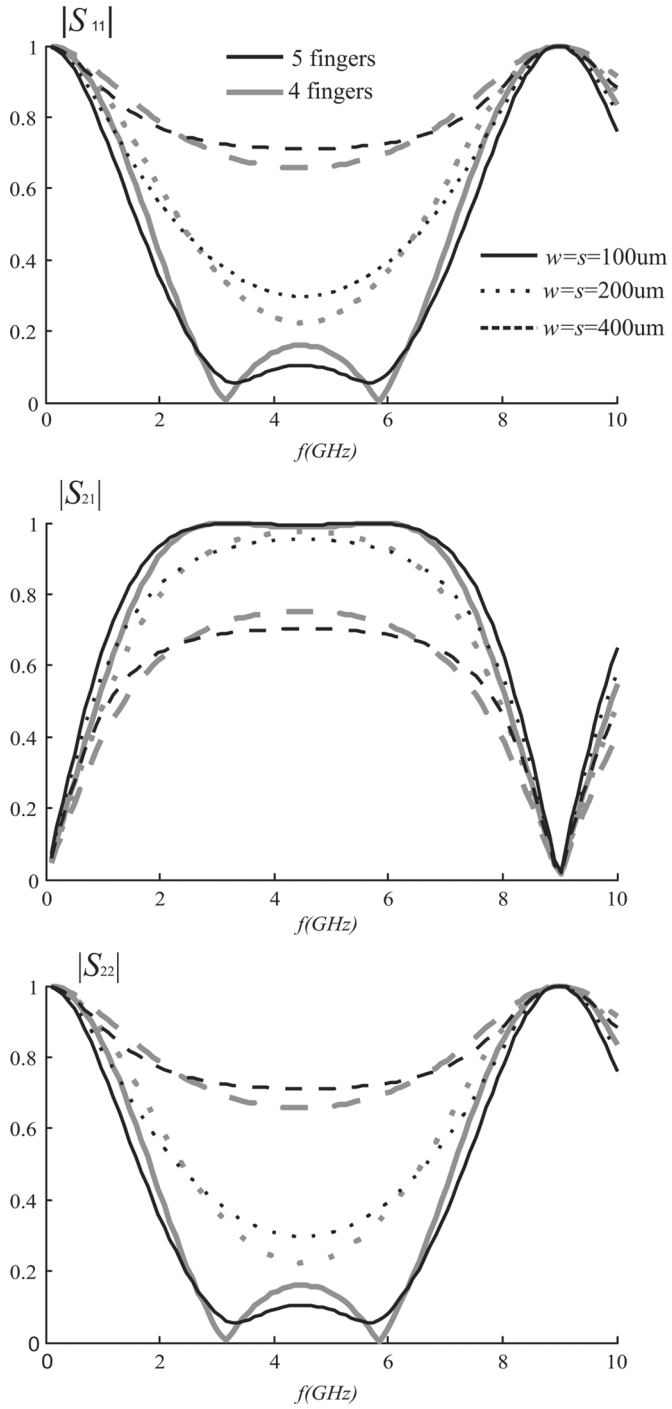

Fig. 8. Calculated scattering matrix elements of microstrip wire-bonded interdigital capacitors (FR4 substrate, thickness: 1.52 mm, relative permittivity: 4.2).

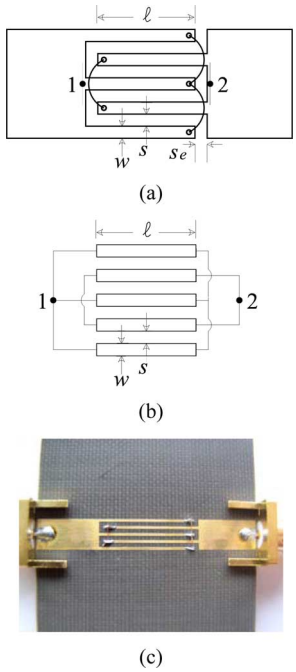

Fig. 9. (a) Layout of the microstrip wire-bonded interdigital capacitor. (b) Drawing of the ideal microstrip transmission line model of the wire-bonded interdigital capacitor. (c) Photograph of the five fingers wire-bonded interdigital capacitor prototype (Rogers Ultralam 2000 substrate, thickness: 1.52 mm, relative permittivity: 2.4).

TABLE I
RELEVANT PARAMETERS OF THE MEASURED WIRE-BONDED INTERDIGITAL CAPACITOR [SEE (20) AND FIG. 9]

Geometrical parameters			
ℓ	w	s	s_e
13.6 mm	0.42 mm	0.61 mm	0.61 mm
Coupled transmission lines model parameters			
n	Z_{0e}	Z_{0o}	θ
0.86	91 Ω	29 Ω	90º
Circuit model parameters			
n	L	C	
0.86	1.80 nH	1.94 pF	

An effective phase velocity can be computed as some type of mean of the phase velocities of all the modes. Once the effective phase velocity has been computed, the performance of the heterogeneous dielectric structure can be determined in the same way as if the dielectric were homogeneous so that all the previous results apply. As shown in Section V, there is an excellent agreement between experimental results and the exact values obtained using an effective permittivity $\varepsilon_{r,\text{eff}}$ computed as the mean value of the effective permittivities of the different propagating modes. In that case, the capacitance matrix is approximated by

$$[C] \approx \frac{1}{2}([C] + \varepsilon_{r,\text{eff}}[C_0]). \tag{26}$$

V. MODEL VALIDATION

A number of multiconductor structures have been designed, simulated, built, and measured to validate the model, which is valid for any number of conductors, even or odd (the analytical model in [3] only supported an even number of conductors, and the reference conductor). The frequency responses of several microstrip wire-bonded interdigital capacitors, obtained with a MoM simulation, are presented in Fig. 8. The results confirm the presence of zero reflection frequencies only for structures narrower than the transmission line of reference impedance.

For the experimental validation, a structure with five conductors, as shown in Fig. 9, has been chosen. Table I shows the relevant dimensions and values of the measured and simulated structures.

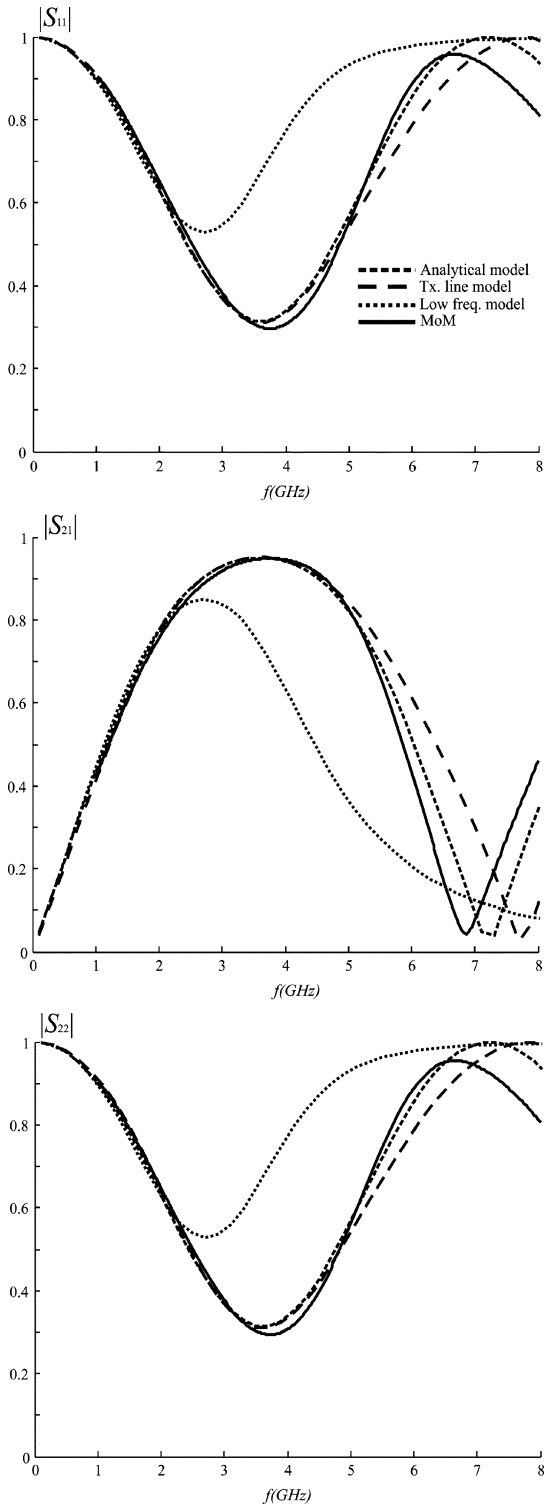

Fig. 10. Calculated scattering matrix elements of the five conductors (plus common) structure described in Table I, computed using models of Figs. 4 and 7, the model in [2], and the MoM (Rogers Ultralam 2000 substrate, thickness: 1.52 mm, relative permittivity: 2.4).

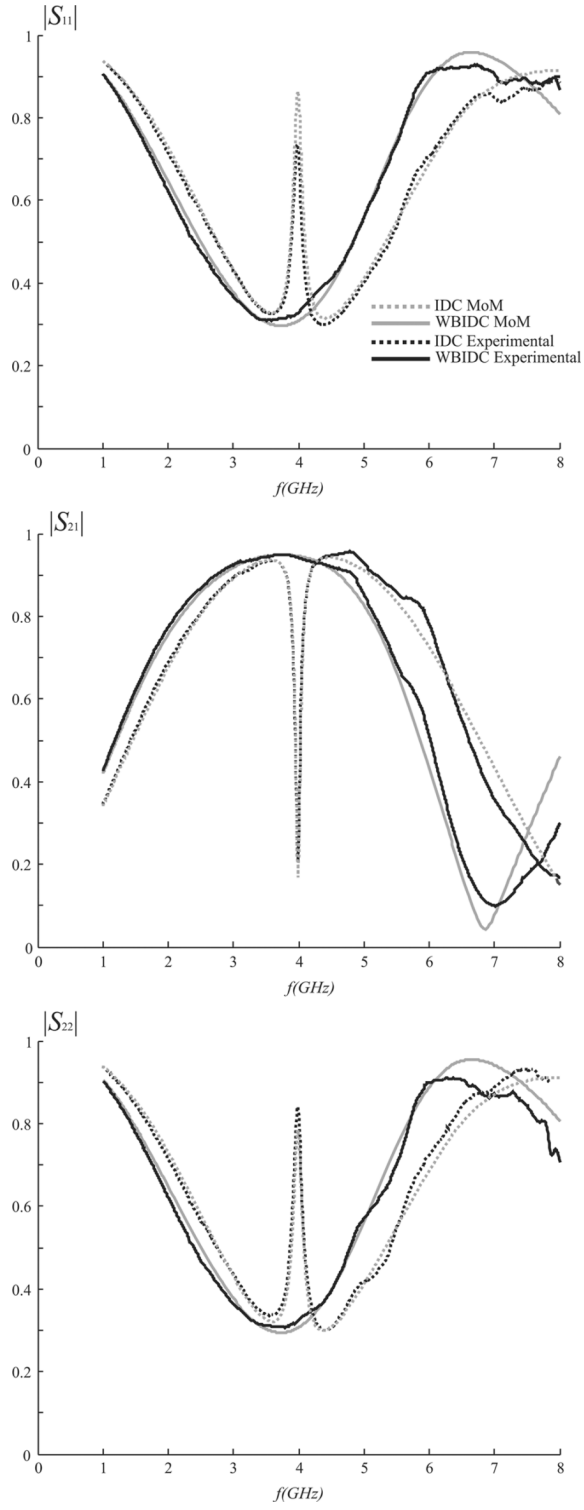

Fig. 11. Measured and calculated (MoM) scattering matrix elements of the same capacitor of Fig. 10. IDC denotes the interdigital capacitor and WBIDC denotes the wire-bonded interdigital capacitor.

To fully validate the model, two sets of graphics are presented. In Fig. 10, the comparison between different models is presented, while Fig. 11 compares calculated to measured results.

Fig. 10 shows the scattering matrix of that structure. The four lines correspond, respectively, to the analytical model, the coupled transmission line model, the low-frequency circuital model, and the MoM analysis of the wire-bonded structure. LINPAR 2.0 was used to calculate the static capacitance matrices of the multiconductor structure [9]. Nonadjacent capacitance terms were included in the simulations. The MoM analysis has been conducted with Agilent's ADS Momentum. It can be

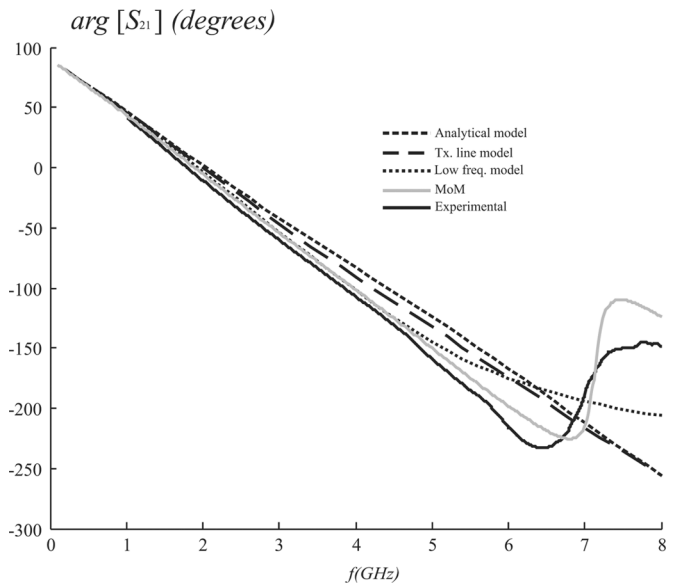

Fig. 12. Calculated and measured argument of the scattering matrix element $S21$ of the five conductors (plus common) structure described in Table I. Magnitude values shown in Figs. 10 and 11.

observed that the model results agree with the full-wave electromagnetic simulation. It must be noted that the simulation results obtained with the aforementioned three methods only consider the ideal (lossless) multiconductor structure, as shown in Fig. 9(b). On the other hand, simulation results obtained with the MoM include the parasitic effects of the junction between the multiconductor structure and the Z_0 access transmission line.

Fig. 11 shows the measured results of the multiconductor structure, with and without bonding wires, of the prototype shown in Fig. 9(c). Fig. 12 shows the computed and measured argument of the S_{21}-parameter. Measurements have been performed with the vector network analyzer Hewlett-Packard HP8510C with thru-reflect-line (TRL) calibration. There is a slight increase in the value of capacitance of the wire-bonded interdigital capacitor, as already explained in [1]. The inherent resonance of the multiconductor structure [10] is eliminated when the bonding wires are connected [1].

Comparing Figs. 10 and 11, it can be seen that the results obtained with the presented model show a very good agreement with the MoM and measured results. Similar agreement between the results obtained using the presented model and the measured results has been obtained with a number of conductors from three to ten (and the reference conductor). Fig. 13 shows the scattering matrix elements of the same structure, but having ten fingers instead of five. The same structure here means that the length of the fingers and the width of the wire-bonded interdigital capacitor are kept constant and equal to those in Table I, which also means that the fingers and slots widths w and s, respectively, decrease with the number of fingers. The values of w and s are indicated in the caption of Fig 13. An identical behavior is found in similar structures with 3–10 fingers. In Fig. 13, the models results are compared to the MoM results. The agreement is good with a slight deviation at higher frequencies, which is mainly due to parasitic effects not considered in the models, as the capacitances of the fingers ends, and the approximation of the value of the effective permittivity of (26). The resonance at high frequencies, evident

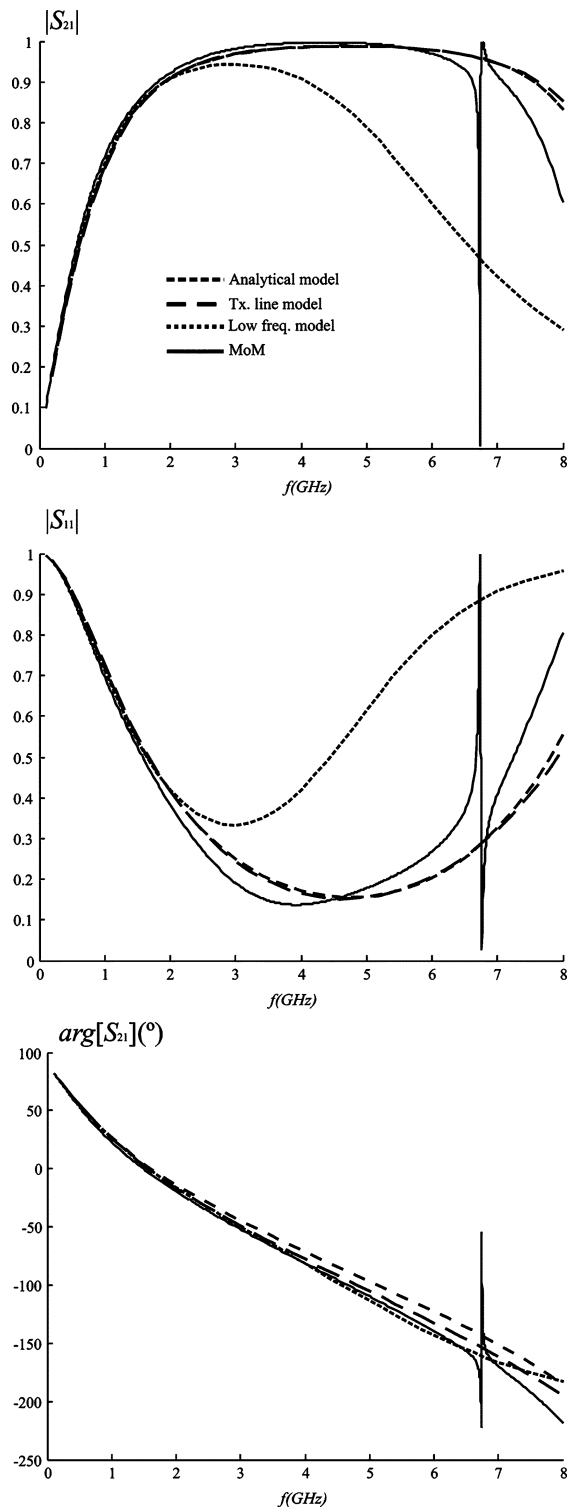

Fig. 13. Calculated scattering matrix elements of the ten conductors (plus common) structure, computed using models of Figs. 4 and 7, the model in [2], and the MoM (Rogers Ultralam 2000 substrate, thickness: 1.52 mm, relative permittivity: 2.4). Fingers and slots widths: $w = s = 239\ \mu$m.

in the MoM simulation of Fig. 13, is due to the inductance of the bonding wires [3].

VI. Conclusion

A particularly useful capacitor device in microstrip technology is the wire-bonded interdigital capacitor, which presents a number

of advantages over the interdigital capacitor. The wire-bonded device can be viewed as a multiconductor guiding structure in a heterogeneous dielectric. In this paper, the exact model of such a structure has been presented. The model is based on the multiport general admittance matrix, and is valid for any number of conductors in the structure. The model allows a designer to compute the two-port admittance matrix of the guiding structure. An equivalent circuit of the structure is presented as well. The model has been validated by means of MoM-based numerical simulation and experimental study. Different microwave substrates and number of fingers have been considered. The model results are in good agreement with the measured results.

REFERENCES

[1] F. P. Casares-Miranda, P. Otero, E. Márquez-Segura, and C. Camacho-Peñalosa, "Wire bonded interdigital capacitor," *IEEE Microw. Wireless Compon. Lett.*, vol. 15, no. 10, pp. 700–702, Oct. 2005.

[2] F. P. Casares-Miranda, E. Márquez-Segura, P. Otero, and C. Camacho-Peñalosa, "Composite right/left-handed transmission line with wire bonded interdigital capacitor," *IEEE Microw. Wireless Compon. Lett.*, vol. 16, no. 11, pp. 624–626, Nov. 2006.

[3] E. Márquez-Segura, F. P. Casares-Miranda, P. Otero, C. Camacho-Peñalosa, and J. E. Page, "Analytical model of the wire bonded interdigital capacitor," *IEEE Trans. Microw. Theory Tech.*, vol. 54, no. 2, pp. 748–754, Feb. 2006.

[4] R. F. Harrington and C. Wei, "Losses on multiconductor transmission lines in multilayered dielectric media," *IEEE Trans. Microw. Theory Tech.*, vol. MTT-32, no. 7, pp. 705–710, Jul. 1984.

[5] C. R. Paul, *Analysis of Multiconductor Transmission Lines*. New York: Wiley, 1994.

[6] E. M. T. Jones and J. T. Bolljhan, "Coupled-strip transmission-line filters and directional couplers," *IRE Trans. Microw. Theory Tech.*, vol. MTT-4, no. 4, pp. 75–81, Apr. 1956.

[7] G. L. Matthaei, L. Young, and E. M. T. Jones, *Microwave Filters, Microwave-Matching Networks, and Coupling Structures*. New York: McGraw-Hill, 1964.

[8] R. Mongia, I. Bahl, and P. Bhartia, *RF and Microwave Coupled-Line Circuits*. Norwood, MA: Artech House, 1999.

[9] A. R. Djordjevic, M. B. Bazdar, T. K. Sarkar, and R. F. Harrington, *LINPAR for Windows: Matrix Parameters for Multiconductor Transmission Lines, Software and User's Manual, Version 2.0*. Norwood, MA: Artech House, 1999.

[10] N. Dib, Q. Zhang, and U. Rhode, "New CAD model of the microstrip interdigital capacitor," *Active and Passive Electron. Compon.*, vol. 27, pp. 237–245, Dec. 2004.

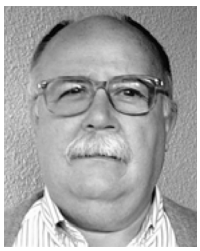

Juan E. Page was born in Madrid, Spain, in 1946. He received the Ingeniero de Telecomunicación and Doctor Ingeniero degrees from the Universidad Politécnica de Madrid, Madrid, Spain, in 1971 and 1974, respectively.

Since 1983, he has been a Professor with the Departamento de Electromagnetismo y Teoría de Circuitos, Universidad Politécnica de Madrid. His research activities include the teaching of electromagnetic and circuit theories and research in the field of computer-aided design (CAD) of microwave devices and systems

Enrique Márquez-Segura (S'93–M'95–SM'06) was born in Málaga, Spain, in April 1970. He received the Ingeniero de Telecomunicación and Doctor Ingeniero degrees from the Universidad de Málaga, Málaga, Spain, in 1993 and 1998, respectively.

In 1994, he joined the Departamento de Ingeniería de Comunicaciones, Escuela Técnica Superior de Ingeniería (ETSI) de Telecomunicación, Universidad de Málaga, where, in 2001, he became an Associate Professor. His current research interests include electromagnetic material characterization, measurement techniques, and RF and microwave circuits design for communication applications.

Francisco P. Casares-Miranda (S'05) was born in Granada, Spain, in 1978. He received the Ingeniero de Telecomunicación degree from the Universidad de Málaga, Málaga, Spain, in 2003, and is currently working toward the Ph.D. degree at the Universidad de Málaga.

Since 2004, he has been a Graduate Student Researcher with the Departamento de Ingeniería de Comunicaciones, Universidad de Málaga. His current research is focused on the analysis and applications of composite right/left-handed metamaterials.

Mr. Casares was the recipient of a Spanish Ministry of Education and Science Scholarship (2004–2008).

Jaime Esteban was born in Madrid, Spain, in 1963. He received the Ingeniero de Telecomunicación and Dr.Eng. degrees from the Universidad Politécnica de Madrid, Madrid, Spain, in 1987 and 1990, respectively.

Since January 1988, he has been with the Departamento de Electromagnetismo y Teoría de Circuitos, Universidad Politécnica de Madrid. In 1990, he became Profesor Interino, and in 1992, Profesor Titular de Universidad. His research topics include the analysis and characterization of waveguides, transmission lines, planar structures and periodic structures, the analysis and design of microwave and millimeter-wave passive devices, and numerical optimization techniques (genetic algorithms and evolution programs). His current research is focused on the analysis and applications of left-handed double-negative, metamaterials and on the biological effects of exposure to RF/microwave fields of radar and modulated signals.

Dr. Esteban was the recipient of a Spanish Ministry of Education and Science Scholarship (1988–1990).

Pablo Otero (S'84–M'93) was born in Seville, Spain, in 1958. He received the Ingeniero de telecomunicación degree from the Universidad Politécnica de Madrid, Madrid, Spain, in 1983, and the Ph.D. degree from the Swiss Federal Institute of Technology at Lausanne (EPFL), Zürich, Switzerland, in 1998.

From 1983 to 1993, he was with the Spanish companies Standard Eléctrica, E.N. Bazán, and Telefónica, where he was involved with communications and radar systems. In 1993, he joined the Universidad de Sevilla, Seville, Spain, where he was a Lecturer for two years. In 1996, he joined the Laboratory of Electromagnetism and Acoustics, EPFL, where he was Research Associate, working under a grant of the Spanish Government. In 1998, he joined the Escuela Técnica Superior de Ingeniería (ETSI) de Telecomunicación, Universidad de Málaga, Málaga, Spain, where he is currently an Associate Professor. His research interests include electromagnetic theory and printed microwave circuits and antennas.

Carlos Camacho-Peñalosa (S'80–M'82) received the Ingeniero de telecomunicación and Doctor Ingeniero degrees from the Universidad Politécnica de Madrid, Madrid, Spain, in 1976 and 1982, respectively.

From 1976 to 1989, he was with the Escuela Técnica Superior de Ingenieros (ETSI) de Telecomunicación, Universidad Politécnica de Madrid, as Research Assistant, Assistant Professor, and Associate Professor. From September 1984 to July 1985, he was a Visiting Researcher with the Department of Electronics, Chelsea College (now King's College), University of London, London, U.K. In 1989, he became a Professor with the Universidad de Málaga, Málaga, Spain. He was the Director of the ETSI de Telecomunicación (1991–1993), and the Vice-Rector (1993–1994), and Deputy Rector (1994) of the Universidad de Málaga. From 1996 to 2004, he was the Director of the Departamento de Ingeniería de Comunicaciones, ETSI de Telecomunicación, Universidad de Málaga. From 2000 to 2003, he was Co-Head of the Nokia Mobile Communications Competence Centre, Málaga, Spain. His research interests include microwave and millimeter solid-state circuits, nonlinear systems, and applied electromagnetism. He has been responsible for several research projects on nonlinear microwave circuit analysis, microwave semiconductor device modeling, and applied electromagnetics.